ARTICLE

Local islet remodelling associated with duct lesion–islet complex in adult human pancreas

Yu-Wen Tien[1] · Hung-Jen Chien[2] · Tsai-Chen Chiang[1] · Mei-Hsin Chung[2,3] · Chih-Yuan Lee[1] · Shih-Jung Peng[4] · Chien-Chia Chen[1] · Ya-Hsien Chou[2,4] · Fu-Ting Hsiao[2] · Yung-Ming Jeng[5] · Shiue-Cheng Tang[2,4]

Abstract

Aims/hypothesis Islets are thought to be stably present in the adult human pancreas to maintain glucose homeostasis. However, identification of the pancreatic intraepithelial neoplasia (PanIN)–islet complex in mice and the presence of PanIN lesions in adult humans suggest that similar remodelling of islet structure and environment may occur in the human pancreas. To identify islet remodelling in a clinically related setting, we examine human donor pancreases with 3D histology to detect and characterise the human PanIN–islet complex.

Methods Cadaveric donor pancreases (26–65 years old, $n = 10$) were fixed and sectioned (350 μm) for tissue labelling, clearing and microscopy to detect local islet remodelling for 3D analysis of the microenvironment. The remodelled microenvironment was subsequently examined via microtome-based histology for clinical assessment.

Results In nine pancreases, we identified the unique peri-lobular islet aggregation associated with the PanIN lesion (16 lesion–islet complexes detected; size: 3.18 ± 1.34 mm). Important features of the lesion–islet microenvironment include: (1) formation of intra-islet ducts, (2) acinar atrophy, (3) adipocyte association, (4) inflammation (CD45+), (5) stromal accumulation (α-SMA+), (6) increase in Ki-67 proliferation index but absence of Ki-67+ alpha/beta cells and (7) in-depth and continuous duct–islet cell contacts, forming a cluster. The duct–islet cell cluster and intra-islet ducts suggest likely islet cell neogenesis but not replication.

Conclusions/interpretation We identify local islet remodelling associated with PanIN–islet complex in the adult human pancreas. The tissue remodelling and the evidence of inflammation and stromal accumulation suggest that the PanIN–islet complex is derived from tissue repair after a local injury.

Keywords 3D pancreatic histology · Human islet · Intra-islet duct · Islet aggregation · Islet cell neogenesis · Pancreatic intraepithelial neoplasia

Abbreviations

α-SMA	α-Smooth muscle actin
CK7	Cytokeratin 7
EUS	Endoscopic ultrasound
PanIN	Pancreatic intraepithelial neoplasia

Yu-Wen Tien and Hung-Jen Chien contributed equally to this work.

✉ Shiue-Cheng Tang
sctang@life.nthu.edu.tw

1 Department of Surgery, National Taiwan University Hospital, Taipei, Taiwan

2 Institute of Biotechnology, National Tsing Hua University, Hsinchu, Taiwan

3 Department of Pathology, National Taiwan University Hospital - Hsinchu Branch, Hsinchu, Taiwan

4 Department of Medical Science, National Tsing Hua University, Hsinchu, Taiwan

5 Department of Pathology, National Taiwan University Hospital, Taipei, Taiwan

Introduction

The bifunctional pancreas consists of both the exocrine parenchyma (acini and ducts) and endocrine islets to facilitate and modulate digestive and metabolic activities. In humans, islets are mostly intra-lobular and surrounded by the acini and ducts, with which the islets have direct contact and indirect neurovascular association to integrate

Research in context

What is already known about this subject?

- In adult humans, glucose homeostasis is maintained by a steady population of islets when individuals have no history of diabetes or pancreatic disease

- Local remodelling of human pancreas, however, is commonly seen in the form of pancreatic intraepithelial neoplasia (PanIN)

- In mouse PanIN, the formation of PanIN–islet complexes with intra-islet ducts indicates associated exocrine and endocrine tissue remodelling in the pancreas

What is the key question?

- Does associated exocrine (duct) and endocrine (islet) tissue remodelling occur in the human pancreas, and what are the key features of the associated remodelling?

What are the new findings?

- In cadaveric donor pancreases, modern 3D histology identified the unique peri-lobular islet aggregation associated with the PanIN lesion

- Main features of the PanIN–islet complex include: formation of intra-islet ducts, acinar atrophy, adipocyte association, inflammation, stromal accumulation, increased cell replication (but absence of Ki-67$^+$ alpha/beta cells), and formation of duct–islet cell clusters

- The duct–islet cell clusters and intra-islet ducts suggest probable islet cell neogenesis but not replication

How might this impact on clinical practice in the foreseeable future?

- Our work suggests that the PanIN–islet complex is derived from tissue repair after a local injury. The PanIN–islet complex provides the morphological context for future genetic and/or molecular marker analyses to investigate islet cell neogenesis in humans

pancreatic structures and functions. In healthy adults, islets are thought to be stably present in the lobules of the pancreas to maintain glucose homeostasis. For example, Saisho et al. examined autopsy pancreases and reported that islet beta cells are well preserved in the adult humans when donors have no history of diabetes or pancreatic diseases [1]. However, local changes in human pancreases are frequently seen in the form of pancreatic intraepithelial neoplasia (PanIN) [2–5]. Importantly, in a mouse model of PanIN, cerulein-induced pancreatic injury leads to the formation of a PanIN–islet complex with intra-islet ducts [6]. This experimental outcome suggests that the associated changes to ducts and islets may be present in the human pancreas, which could affect local islet homeostasis.

Clinically, although PanIN is linked to cancer [3], the overwhelming majority of PanIN lesions are stable. The origin of PanIN in humans is still under debate but has been linked to acinar-to-ductal metaplasia (with *Kras* mutation) and/or local pancreatic injury (e.g. pancreatitis induced by local duct obstruction) [3–5, 7–10]. In mice, duct obstruction induced by partial duct ligation leads to lobular injury, inflammation and tissue regeneration, in which evidence of islet alpha and beta cell regeneration, including beta cell neogenesis, has been reported [11–13].

Yet, conflicting results showing no beta cell neogenesis have also been reported ([14, 15], via lineage tracing analysis), creating controversy on the intricate processes of pancreatic and islet regeneration after injury. In humans, the situation is further complicated by significant differences between the mouse and human pancreases in macrostructure (assembly of soft lobules vs solid organ), islet cytoarchitecture and islet cell physiology to extrapolate likely human islet regeneration from experimental conditions [16–18]. Thus, to investigate islet remodelling in the human PanIN microenvironment, careful examination of islets and ducts with multiplex and multidimensional signals is crucial to identify and confirm the associated tissue remodelling in a novel environment.

Recent advances in modern 3D histology with tissue clearing and its application to characterise the islet neurovascular connections in mouse and human pancreases [19–26] provide an enabling approach to simultaneously detect and characterise the PanIN and islet microenvironment with high definition. Microscopically, when the human pancreas becomes transparent, the acinar, duct and islet structures and neurovascular networks are visualised in a 3D space continuum, providing details of the exocrine–endocrine integration [22–25]. In this research we prepared

transparent cadaveric donor pancreases for panoramic and in-depth imaging of duct and islet remodelling to investigate the human PanIN–islet complex. The results of morphological and quantitative analyses of the human PanIN–islet complex are presented and discussed in this report.

Methods

Human pancreatic specimens Human pancreases were obtained from ten cadaveric donors with normal HbA$_{1c}$, amylase and lipase levels. Collection and use of human tissues were approved by the Institutional Review Board of National Taiwan University Hospital. Donor pancreases were first cut to separate the head, body and tail of the organ and then into strips (~1.5 cm in width) before being fixed in 4% (vol./vol.) formaldehyde for 2 days (4°C). The fixed tissues were washed in PBS for 4 days (4°C) and then sectioned to 350 μm specimens by vibratome before being transferred to 0.1% (vol./vol.) paraformaldehyde for preservation (4°C) [22]. The head, body and tail of each pancreas were individually analysed (1.5–2 cm^3 of each region). Table 1 lists the sex, age, BMI, HbA$_{1c}$ level and cause of death of the donors, and location of the detected peri-lobular islet aggregation.

Pancreatic tissue labelling Before immunolabelling, the specimens were immersed in 2% Triton X-100 solution for 2 h at 15°C for permeabilisation. Eleven different primary antibodies were used to immunolabel the pancreatic tissues. The following antibodies were used: mouse anti-insulin (sc-8033_AF488, Santa Cruz, Dallas, TX, USA), mouse anti-glucagon (ab10988, Abcam, Cambridge, MA, USA), rabbit anti-glucagon (ab92517, Abcam), rabbit anti-cytokeratin 7 (CK7; ab68459,

Abcam), mouse anti-α-smooth muscle actin (α-SMA; MS-113-P1, Thermo, Fremont, CA, USA), rabbit anti-PGP9.5 (ab108986, Abcam), mouse anti-CD31 (MS-353-S1, Thermo), mouse anti-podoplanin (clone D2-40; 916602, BioLegend, San Diego, CA, USA), rabbit anti-Ki-67 (ab15580, Abcam), mouse anti-Ki-67 (61-0078, Genemed, Torrance, CA, USA) and mouse anti-CD45 (NCL-L-LCA, Leica Biosystems, Buffalo Grove, IL, USA). Before applying the antibodies, tissue sections were rinsed in PBS. This was followed by a blocking step, incubating the tissue with blocking buffer (2% Triton X-100, 10% normal goat serum, and 0.02% sodium azide in PBS). The primary antibody was then diluted in dilution buffer (1:100, 0.25% Triton X-100, 1% normal goat serum, and 0.02% sodium azide in PBS) to replace the blocking buffer and incubated for 2 days at 15°C to label tissue or cellular structures. Electronic supplementary material (ESM) Table 1 summarises the immunostaining reagents/dilutions used in the figures and ESM figures.

Alexa Fluor (AF)-488, -546, and -647 conjugated secondary antibodies (raised in goat; 1:200, Thermo) were used in combination to reveal the immunostained structures. Negative staining controls were prepared by omitting the primary antibody in the staining reagent. DAPI or SYTO 16 (Thermo) staining was performed to reveal nuclei. To maximise photon penetration in deep-tissue fluorescence imaging, the labelled specimens were transferred to an aqueous tissue-clearing solution with high refractive index (RapiClear 1.52 solution, SunJin Lab, Hsinchu, Taiwan) overnight and then immersed in fresh RapiClear solution for one day before being imaged via transmitted light and confocal microscopy.

Deep-tissue 3D confocal microscopy Imaging of the tissue structure was performed with a Zeiss LSM 800 confocal microscope (Carl Zeiss, Jena, Germany) using a tile-scan

Table 1 Donor information

Donor	Sex	Age (years)	BMI	HbA$_{1c}$,% (mmol/mol)	Cause of death	Location of detected peri-lobular islet aggregation
1	Female	26	22.2	5.2 (33)	Cerebral hypoxia	Tail
2	Male	37	26.3	5.5 (37)	Traumatic brain injury	Head and body
3	Female	40	23.8	5.6 (38)	Cerebrovascular/stroke	Head and tail
4	Male	50	20.3	5.6 (38)	Brain tumour	Tail
5	Female	51	19.8	5.3 (34)	Cerebrovascular/stroke	Head (two locations) and body
6	Female	51	22.8	5.4 (36)	Cerebrovascular/stroke	Head, body and tail
7	Male	53	28.0	6.0 (42)	Subarachnoid haemorrhage	Tail
8[a]	Male	54	23.2	5.4 (36)	Cerebral hypoxia	None
9	Female	64	27.1	5.4 (36)	Cerebrovascular/stroke	Head and tail
10	Female	65	18.2	6.0 (42)	Cerebrovascular/stroke	Body

[a] Peri-lobular islet aggregation and formation of PanIN–islet complex are identified in all donors except donor 8

mode with automatic image stitching. The laser-scanning process was operated using the multi-track scanning mode to acquire signals, including transmitted light signals, which reveal the pancreatic lobules and infiltrated adipocytes. The AF-647-labelled structures were excited at 633 nm and the fluorescence was collected by a 650–710 nm filter. The AF-546-labelled structures were excited at 543 nm and the signals were collected by a 560–615 nm filter. The AF-488-labelled structures were excited at 488 nm and the fluorescence was collected by a 500–550 nm filter. Fluorescence signals in the figures are pseudo-coloured. ESM Table 2 summarises the colour codes for different markers in the figures and ESM figures.

3D/2D integrative histology When a duct lesion–islet complex was detected in a 350 μm tissue section via 3D imaging, the section was next processed by dehydration, embedding and microtome sectioning to generate 4 μm paraffin slices for H&E staining (Leica Autostainer XL). H&E-stained specimens were examined using the same Zeiss microscope for side-by-side comparison of the 3D fluorescence and 2D H&E micrographs to confirm the PanIN lesion (e.g. Fig. 1d–f). Once confirmed, multiplex signals from the same microenvironment were further acquired from adjacent tissue sections via standard immunohistochemistry (4 μm sections; Bond Polymer detection kit, Leica Biosystems, DS9800/DS9390) and 3D histology (350 μm sections) with the markers summarised in ESM Table 1 to analyse the PanIN–islet microenvironment.

Image projection and analysis Avizo 6.2 image reconstruction software (VSG, Burlington, MA, USA), Zen software (Carl Zeiss) and LSM 510 software (Carl Zeiss) were used for projection, signal segmentation, noise reduction and analysis of the confocal images. Signal segmentation for quantification of tissue density is illustrated in Juang et al. [27]. Briefly, feature extraction and image segmentation for calculation of the alpha cell (or lymphatic vessel) density were performed using the Label Field function of Avizo to collect the pixels in the area of interest (lesion–islet complex; e.g. the arbitrary oval in Fig. 1a) and the associated glucagon (or D2–40) signals. Areas in the same tissue map but >1 mm away from the lesion–islet complex were used as the control (normal pancreas). Pixels with the glucagon (or D2–40) signals were divided by those of the area of interest ×100% to estimate the alpha cell (or lymphatic vessel) density. The Ki-67 proliferation index (%) was defined as the percentage of nuclei in the area of interest (lesion–islet complex or normal pancreatic lobule) labelled with Ki-67. The same tissue labelling, imaging and quantification processes were conducted on the comparable pancreatic sections to compare the tissue densities and proliferation indexes on the same basis.

Statistical analysis Quantitative values are presented as means ± SD with the distribution of data points. Statistical differences were determined by the unpaired Student's t test. Differences between groups were considered statistically significant when $p < 0.05$.

Results

**Peri-lobular islet aggregation and duct lesion–islet complex in human pancreas** Human islets are primarily intra-lobular and scattered in the pancreatic parenchyma. However, in our scanning of the transparent donor pancreas labelled with ductal (CK7) and islet (glucagon) markers (Fig. 1a and ESM Fig. 1; optically cleared specimen [22]), the unique peri-lobular islet aggregation around the duct lesion caught our attention for detailed investigation. Among the ten analysed donor pancreases (Table 1; age: 26–65 years old; BMI: 18.2–28.0), nine (90%) were detected to have local islet aggregation and all of the aggregations (100%) were associated with the PanIN-1A/B lesions (confirmed by H&E images; see [2] for details). Note that, for morphological and quantitative analyses of the lesion–islet complex, an arbitrary boundary (e.g. an oval in Fig. 1a and ESM Fig. 1) was used to enclose the aggregated islets and the PanIN lesion for illustration and to quantify the tissue components. Overall, 16 duct lesion–islet complexes (size: 3.18 ± 1.34 mm) were detected in the ten pancreases.

Compared with the normal pancreas (normal lobular architecture; >1 mm away from the lesion–islet complex), the lesion–islet complex had an 8.9-fold ($p < 0.001$) increase in islet density (Fig. 1b; inside the arbitrary oval boundary in Fig. 1a and ESM Fig. 1; major axis at 1.5–5 mm). From the transmitted light signals (Fig. 1a), we also identified that 88% of the lesion–islet complexes were associated with adipocytes, either inside the complex or at the periphery or both (Fig. 1c).

To confirm the lesion–islet complex, a parallel presentation of the high-resolution 2D image (Fig. 1d), 3D projection (Fig. 1e), and clinical H&E micrograph (Fig. 1f) was used to illustrate and cross-validate the tissue remodelling. In addition to islet aggregation, Fig. 1d–f also reveals the loss of acini (or acinar atrophy) in the microenvironment, which is similar to the lobular atrophy previously reported around PanIN [28]. In quantification, while only a small percentage of the analysed pancreas (0.32 ± 0.30%) was found with the lesion–islet complex, a marked 2.32 ± 1.90% of the observed islets were inside the complex (Fig. 1g). The result reflects that the complex disproportionately includes more endocrine islets than exocrine tissues owing to islet aggregation.

It is worthwhile noting that cross-validation of lesion–islet complexes was made possible by the integration of 3D confocal imaging with microtome-based H&E histology (Fig. 1d–

Fig. 1 Peri-lobular islet aggregation and duct lesion–islet complex in human pancreas. (**a**) Map of pancreas revealing islet aggregation and lesion–islet complex (representative image). Tile scanning and image stitching were used to generate the tissue map (overlay of fluorescence and transmitted light signals; the latter was used to identify fatty infiltration in the transparent specimen [22]). Magenta, glucagon staining of islets; green, CK7 staining of duct epithelium; white, nuclear staining; scale bar, 2 mm. (**b**) Increase in islet density in the lesion–islet complex (vs normal pancreas). Pixels occupied by glucagon$^+$ alpha cells divided by pixels (area) of interest (e.g. arbitrary oval in **a**) ×100% was used to estimate the islet density. Areas in the same tissue map but >1 mm away from the lesion–islet complex were used as the control (normal pancreas). ***$p < 0.001$. (**c**) Percentage of lesion–islet complexes associated with adipocytes. All 16 lesion–islet complexes identified in the ten donors were used in the analysis. (**d**–**f**) PanIN confirmation and cross-validation of PanIN–islet complex via parallel presentation of fluorescence, transmitted light and H&E signals. Oval, PanIN–islet complex; asterisks, adipocytes; P, parenchyma; blue, insulin; magenta, glucagon; green, CK7; white, nuclei; scale bar, 500 μm. (**g**) Percentage of analysed pancreas with PanIN–islet complex and percentage of observed islets inside the PanIN–islet complex. All ten donor pancreases were used in the analysis, including donor 8 (Table 1)
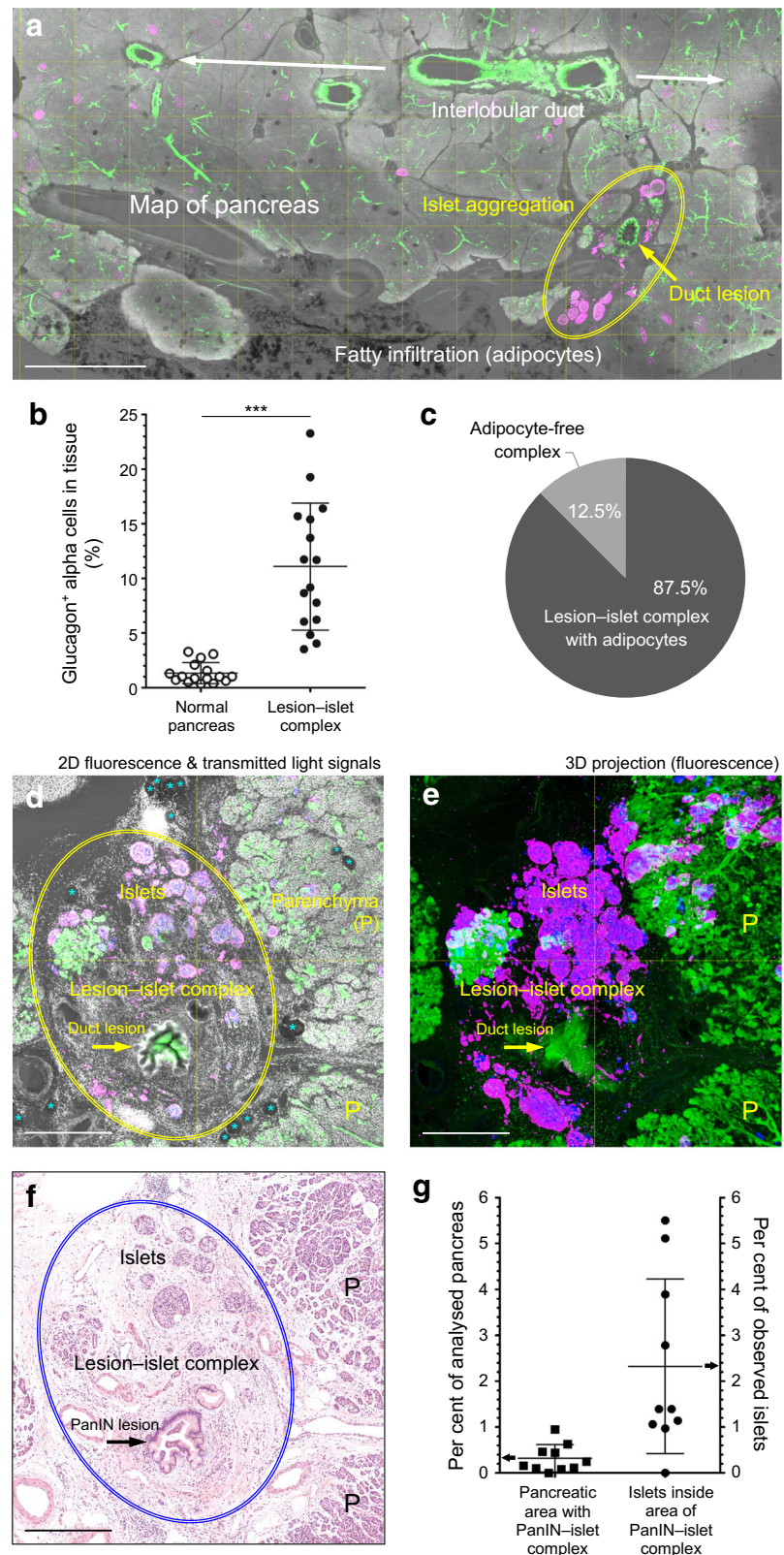
f). The z-axis alignment between the confocal image stack and the microtome sections provides a side-by-side comparison of the multiplex signals (ESM Video 1), including the

transmitted light, multi-channel fluorescence and H&E (ground truth tissue information for PanIN identification [2]) signals, to depict and confirm a complex environment.

Fig. 2 Associated changes of islet and duct in the PanIN–islet microenvironment. (**a**–**c**) Formation of intra-islet ducts in lesion–islet microenvironment. (**a**) Map of pancreas and enlarged intra-islet ducts (inset, yellow arrows). Blue, insulin; magenta, glucagon; green, CK7; white, nuclei; scale bar, 1 mm (inset, 100 μm). (**b**, **c**) Second example of intra-islet ducts in 2D image and 3D projection; scale bar, 100 μm. (**d**, **e**) High-resolution images of epithelium–islet cell association (representative image; scale bar, 100 μm). (**d**) Two features of the association: (1) islet cells attaching to the basal domain of epithelium (arrows) and (2) epithelium expressing endocrine marker. (**e**) Endocrine cell strip along the longitudinal direction of duct (number 3). Blue, insulin; magenta, glucagon; green, CK7; white, nuclei. (**f**) Percentage of islets with intra-islet duct in lesion–islet complex. (**g**) Increase in percentage of ductal cells expressing endocrine marker (insulin or glucagon) in lesion–islet complex vs normal pancreas (>1 mm away from the complex). Inter- or peri-lobular ductal cells in the nine donor pancreases with the lesion–islet complex were used in the analysis. ***$p < 0.001$
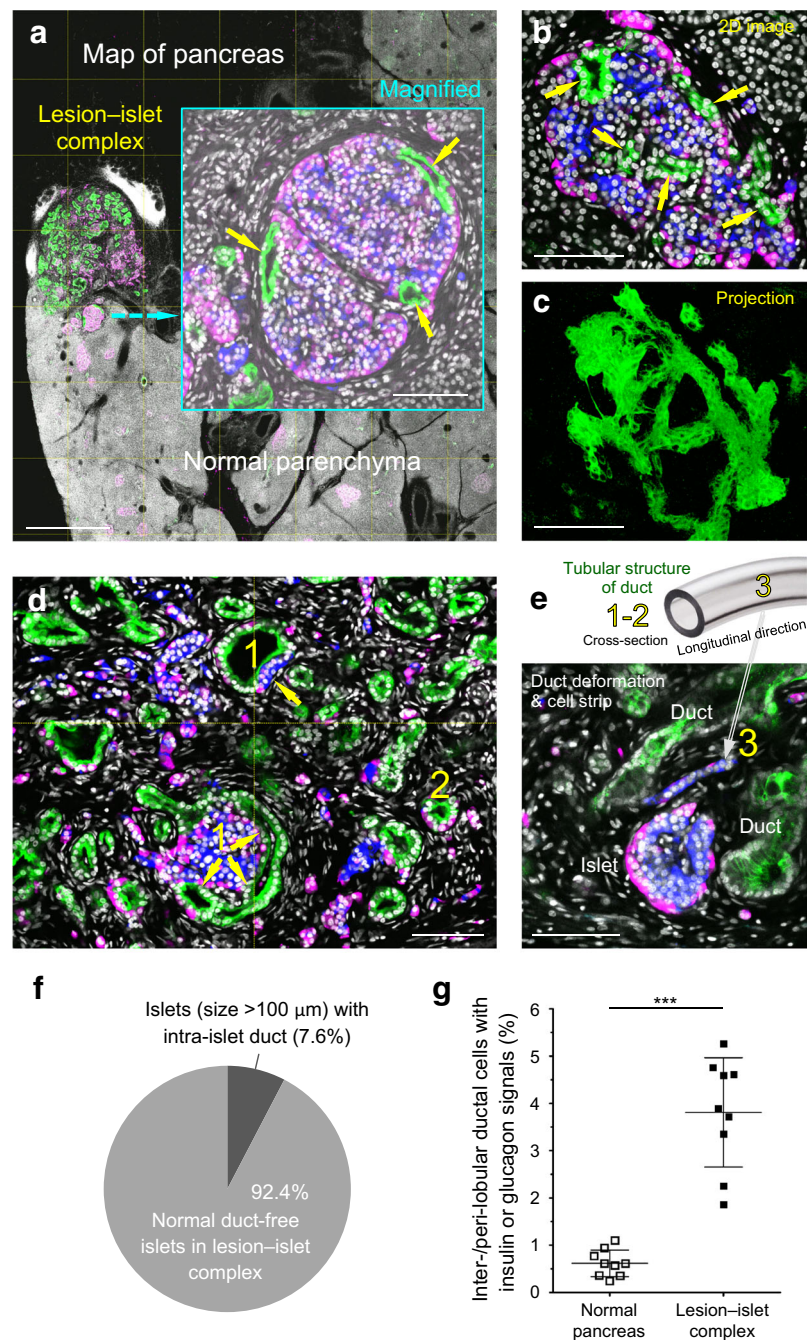
Associated changes of islet and duct in lesion–islet microenvironment We next zoomed into the lesion–islet microenvironment to reveal details of islet and duct remodelling. First, using quadruple staining of glucagon, insulin, CK7 and nuclei, we detected the localised formation of intra-islet ducts (Fig. 2a–c and ESM Fig. 2). In addition, high-resolution images of the microenvironment reveal: (1) the alpha and beta cells attaching to the basal domain of the duct epithelium; and (2) the duct epithelium expressing the islet cell markers glucagon and insulin (Fig. 2d). In addition, strips of glucagon$^+$

and insulin$^+$ cells can be identified along the longitudinal direction of the tubular epithelium (Fig. 2e), differing from the normal spherical structure of the islet.

In quantification, 7.6% of the islets (size >100 μm) observed in the lesion–islet complex were identified as having intra-islet ducts (Fig. 2f; 22 of 288 islets with CK7$^+$ epithelium reaching the core), while no intra-islet ducts were identified in the normal pancreatic lobules (1150 islets examined). In the same microenvironment, we detected a 6.2-fold ($p < 0.001$) increase in the percentage of ductal cells labelled with insulin or glucagon compared
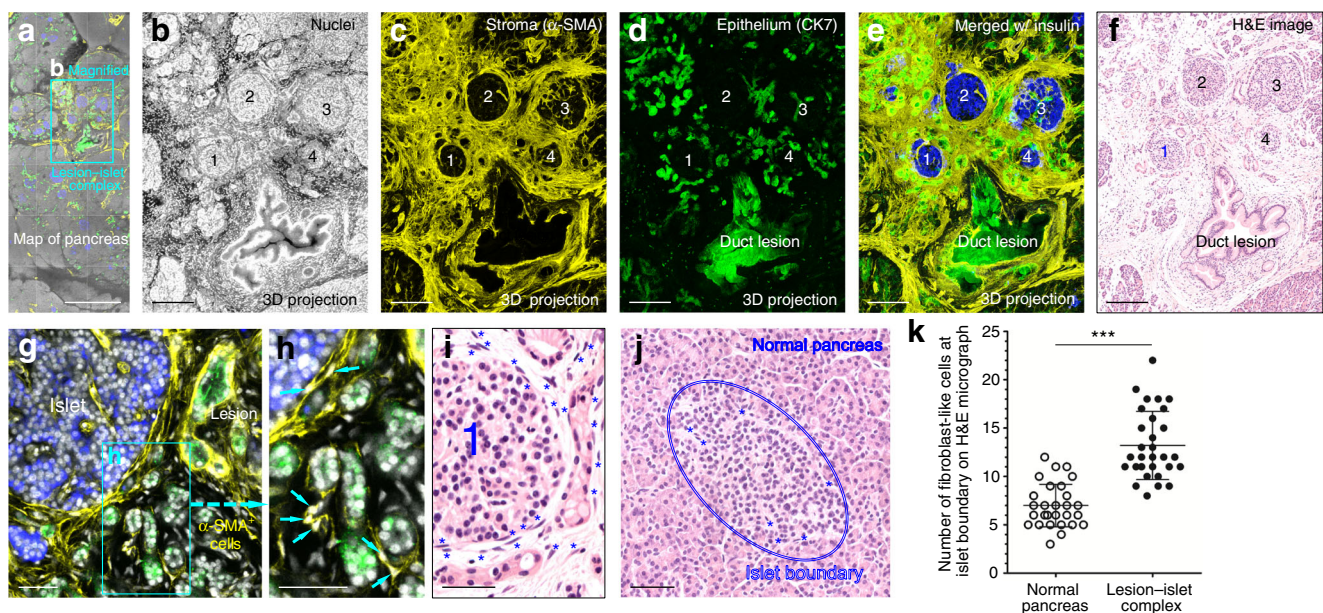
Fig. 3 Stromal cell accumulation associated with the PanIN–islet complex. (**a–f**) α-SMA staining reveals stromal accumulation in lesion–islet microenvironment. (**a**) Map of pancreas (representative image; scale bar, 1 mm). An enlarged PanIN–islet complex (box) is presented in (**b–f**) (3D fluorescence and H&E images; scale bar, 200 μm) to identify and confirm the islet aggregation and PanIN lesion. Numbers 1–4 indicate four large islets around the lesion. The α-SMA⁺ stroma (yellow) fills the space between islets and lesion. Blue, insulin; green, CK7; white, nuclei. (**g–j**) Association of α-SMA⁺ myofibroblasts with islet and duct lesion. The box in (**g**) is enlarged in (**h**) to reveal the cell bodies (arrows) and processes of α-SMA⁺ myofibroblasts embracing the duct lesion and islet. Yellow, α-SMA; blue, insulin; green, CK7; white, nuclei. (**i**) H&E micrograph to confirm the fibroblast-like cells (asterisks, elongated nuclei); (1) indicates the number 1 islet in (**b–f**). (**j**) Acinar–islet association in normal pancreas (vs stromal–islet association in (**i**); asterisks, fibroblast-like cells at islet boundary. Scale bar in (**g–j**), 50 μm. (**k**) Increase in peri-islet fibroblast-like cells in lesion–islet complex vs normal pancreas (>1 mm away from the complex). 30 islets (150–200 μm) on the H&E micrographs in each condition were used in the analysis. ***$p < 0.001$

with that of the normal pancreas (Fig. 2g). Overall, these results indicate a locally diminished tissue boundary between ducts and islets in the lesion–islet complex.

Stromal cell accumulation associated with PanIN–islet complex The stromal cells of fibroblasts and myofibroblasts (stellate cells) are sparse and quiescent in the normal pancreas; however, they become activated and proliferative in pancreatic injury and inflammation (e.g. pancreatitis), causing fibrosis [29, 30]. In Fig. 3a–f and ESM Fig. 3, we integrate 3D fluorescence and 2D H&E signals to reveal that a similar phenomenon of fibrosis (or stromal cell accumulation) occurs in the PanIN–islet complex. Quadruple staining of α-SMA (fibrosis marker), CK7, insulin and nuclei identifies a prominent presence of α-SMA⁺ myofibroblasts around both the duct lesion and the aggregated islets, forming a triad of stroma, PanIN and islet to replace the normal pancreatic components of acinus, duct and islet in the lobule.

The enlarged images of the microenvironment further show that the cell bodies and processes of α-SMA⁺ myofibroblasts embrace the basal domain of the duct lesion and islet (Fig. 3g,h), which is confirmed by the elongated nuclei in the H&E micrograph (Fig. 3i). The result indicates the change in the immediate microenvironment of the aggregated islets compared with that of the normal islets, in which the islets

are scattered in the parenchyma and surrounded by acini (Fig. 3j; note that, unlike mouse islets, human islets do not have a glial sheath [22]). Quantitative analysis of the H&E images in the lesion–islet microenvironment shows a 1.9-fold ($p < 0.001$) increase in the number of fibroblast-like cells at the islet boundary compared with that of the normal pancreas (Fig. 3k), confirming the peri-islet stromal cell accumulation. However, because H&E staining is nonspecific, this analysis cannot distinguish between fibroblasts, myofibroblasts, glia and peri-arteriolar smooth muscle cells in the microenvironment to specify the cellular response.

Evidence of tissue injury and regeneration in lesion–islet microenvironment Both the intra-islet ducts identified in Fig. 2a–c and the peri-PanIN fibrosis revealed in Fig. 3 suggest that a local pancreatic injury could have occurred, leading to tissue remodelling and regeneration after the injury. To support this concept of pancreatic injury and regeneration, we used the signals of lymphatic vessels (D2–40⁺), leucocyte (CD45⁺), and Ki-67 to investigate the inflammatory response and cellular replication in the lesion–islet complex (Fig. 4a–f). Three features of the microenvironment are revealed in the analysis: (1) increase in lymphatic vessel density (or lymphangiogenesis) in the lesion–islet complex vs the normal pancreas (3.2-fold, $p < 0.01$; Fig. 4a–c and ESM Video 2); (2) peri-lesional
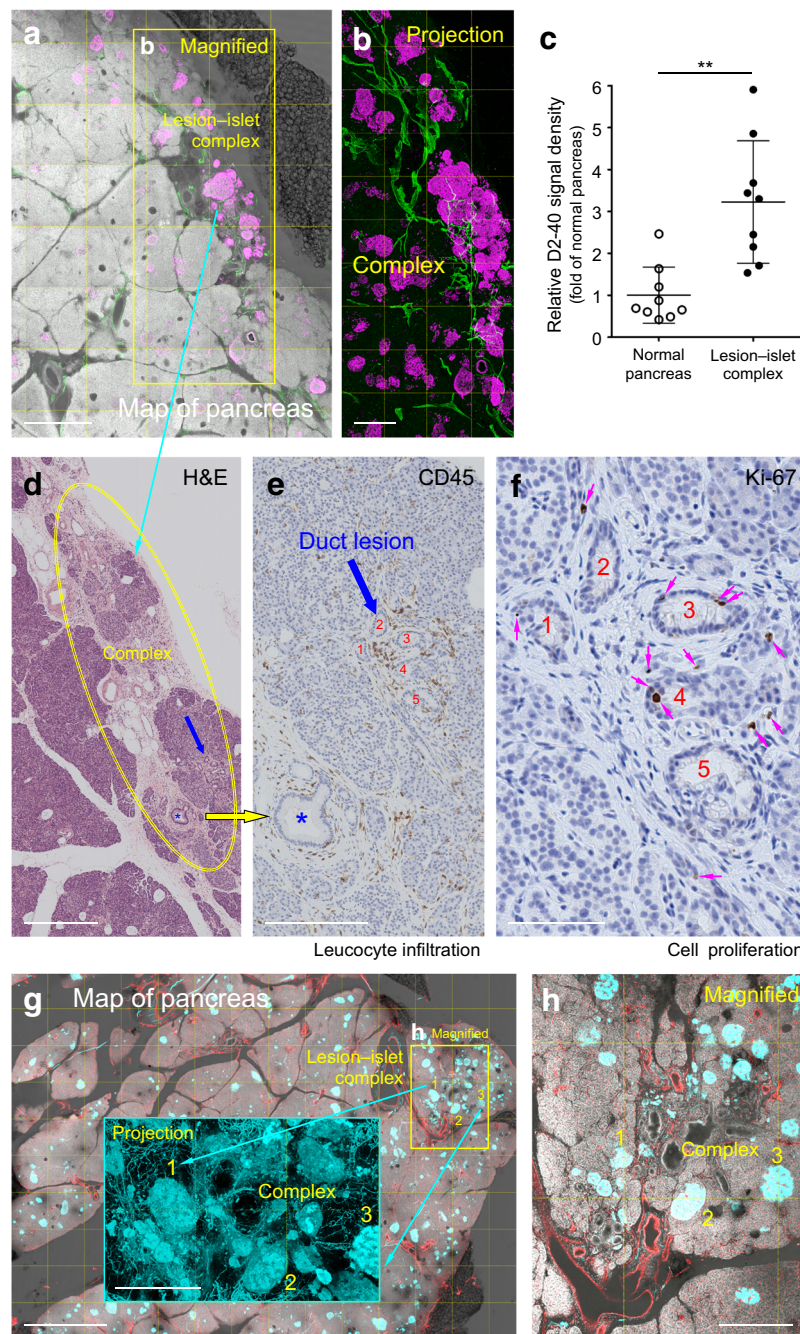
Fig. 4 Lymphatic network, leucocyte infiltration, cell proliferation and neurovascular association in the PanIN–islet microenvironment. (**a–c**) Increase in lymphatic vessel density in lesion–islet complex (vs normal pancreas, >1 mm away from the complex). (**a**) Map of pancreas (representative image; scale bar, 1 mm). The box in (**a**) is magnified in (**b**; scale bar, 500 μm) to show the lymphatic network (D2–40 staining, green). The same microenvironment is examined in (**d–f**). Magenta, glucagon. (**c**) D2–40 signals in the nine pancreases with the lesion–islet complex were used in the analysis. **$p < 0.01$. (**d–f**) Clinical H&E, CD45 and Ki-67 examination of lesion–islet microenvironment. (**d–f**) Images are derived from serial paraffin sections adjacent to (**a**) (cyan arrow). The oval in (**d**) indicates the lesion–islet complex. Areas around

the asterisk (duct) and blue arrow (duct lesion, PanIN-1A [2]) are enlarged in (**e**) to identify peri-lesional leucocyte infiltration (aggregation of CD45 signals). Scale bar in (**d, e**), 500 μm. Numbers 1–5 (duct lesion) in (**e**) are further enlarged in (**f**; scale bar, 100 μm) to reveal the Ki-67+ proliferating cells (arrows) in the microenvironment. (**g, h**) Neurovascular association of lesion–islet complex (representative image). Cyan, PGP9.5 (neuroendocrine marker, nerves and islets); red, CD31 (blood vessels). The yellow box in (**g**) is magnified in (**h**) to identify the peri-lesional islets (e.g. islets numbered 1–3) and neurovascular tissues. Scale bar in (**g**), 2 mm; scale bar in (**h**), 500 μm. The neuro-insular network is enlarged in inset (scale bar, 500 μm) to present the condensed nerve fibres in the lesion–islet complex

leucocyte infiltration (inflammation, aggregation of CD45 signals; identified in all nine analysed lesion–islet complexes)

(Fig. 4d,e); and (3) prominent Ki-67+ cell proliferation in the lesion–islet microenvironment (Fig. 4f).

We also assessed the neurovascular networks in this microenvironment via paired PGP9.5 (neuroendocrine marker) and CD31 (endothelial marker) staining. Figure 4g,h shows that the lesion–islet complex is surrounded by condensed nerve fibres and blood vessels (note that PGP9.5 staining also labels islets), confirming islet aggregation and a rich neurovascular supply to this proliferative environment.

Absence of islet alpha and beta cell proliferation in lesion–islet complex The tissue inflammation and marked cell proliferation in the lesion–islet microenvironment (Fig. 4a–f) raise a critical question: does islet cell replication and/or neogenesis occur in this environment? To address the first part of this question, we applied quadruple staining using Ki-67, glucagon, insulin and nuclei to investigate the identity of proliferating cells. As can be seen in Fig. 5a–e, the Ki-67$^+$ cells are both inside and around the aggregated islets and ducts. The high-resolution images (Fig. 5b–e) and videos (ESM Video 3 and 4) show that, although the Ki-67$^+$ nuclei are adjacent to the alpha and beta cells, they are not enclosed by glucagon or insulin signals, indicating the absence of alpha and beta cell replication.

Next, using the Ki-67 proliferation index (% of cells in proliferation), we identified a 3.5-fold ($p < 0.001$) increase in cell replication in the lesion–islet complex vs the normal pancreatic lobule (Fig. 5f). Among the proliferating cells in the lesion–islet complex, 7.2% and 21.3% of them were associated with the islet and duct, respectively (Fig. 5g). In the duct, a subgroup of the proliferating cells (2.1%) was residing next to the glucagon$^+$ or insulin$^+$ cells. Overall, 9.3% of proliferating cells in the lesion–islet complex were adjacent to the immunoreactive alpha or beta cells, while no Ki-67$^+$ alpha or beta cells were identified.

In-depth and continuous duct–islet cell contacts and integration in lesion–islet complex Regarding the second part of the above question, in mice beta cell neogenesis has been identified by lineage tracing analysis of the injured pancreas induced by partial duct ligation [12]. Interestingly, despite the experimental nature of this tracing analysis, the pancreatic injury led to the formation of duct (cytokeratin$^+$)–islet (insulin$^+$) cell clusters, which in humans are notably identified in the PanIN–islet complex. As can be seen in Fig. 6a–e, we used the pancreas map to specify the location of the duct lesion–islet complex in the donor pancreas. Zooming into the area of interest, the multiplex (CK7, glucagon, insulin and nuclear) and in-depth signals identify the formation of duct (CK7$^+$)–islet (glucagon$^+$ and/or insulin$^+$) cell clusters associated with the duct epithelium (Fig. 6f–g and Fig. 6h–i; size of cell cluster: 76 ± 20 μm, $n = 12$). ESM Figs 4–6 provide additional examples of the continuous duct–islet cell contacts and integration in the lesion–islet complex. The duct–islet cell clusters, together

with the islet aggregation (Fig. 1) and intra-islet ducts (Fig. 2), highlight the histological features of PanIN–islet complexes in the adult human pancreas.

Discussion

Although islets are thought to be stably present in the adult human pancreas to maintain glucose homeostasis, in this research we identify local islet remodelling in the PanIN–islet complex via high-resolution tissue imaging. Histologically, PanIN is a well-defined duct lesion and commonly seen in the human pancreas [3–5]. However, prior to this research, PanIN-associated islet remodelling could not be globally examined in a clinically related setting owing to the technical constraint of microtome-based 2D histology. Here, using the transparent pancreas [22], we combine modern 3D and classic 2D histology to examine the human PanIN–islet complex in a global and integrated fashion.

Using high-resolution images, we identified perilobular islet aggregation associated with PanIN, which contributes to a local increase in islet density (Fig. 1a,b). This phenomenon appears to be caused in part by acinar atrophy around PanIN (Fig. 1d–f and [28]). However, acinar atrophy cannot explain the formation of intra-islet ducts (Fig. 2a–c) and duct–islet (alpha/beta) cell clusters (Fig. 6) in the lesion–islet complex. These two unique forms of duct–islet cell integration suggest that islet cell neogenesis (not replication, as we can see from absence of Ki-67$^+$ alpha and beta cells, Fig. 5) may have contributed to the increase in islet density, although lineage-tracing analysis would be needed to demonstrate the neogenic process more definitely.

Previously, the formation of intra-islet ducts has been detected in rodent models, children, and pancreatic cancer patients [6, 20, 31–33]. In mice, intra-islet ducts have been reported to give rise to insulin$^+$ cells [33]. In this study, the epithelial ingrowth to islets is particularly similar to that found in $Kras^{G12D}$ mutant mice when treated with cerulein to induce pancreatitis and PanIN [6]. Taking together these developmental and injury conditions and the trophic effect of insulin [34], we suspect that the local increase in islet density (Fig. 1a,b) and the intimate islet–duct contacts (Fig. 2a-d and Fig. 6) are intrinsic responses of human pancreas to facilitate tissue repair after a PanIN-associated injury. This concept of tissue injury, inflammation and repair is also supported by the findings of stromal cell accumulation (Fig. 3), increase in lymphatic vessel density (Fig. 4a–c), leucocyte infiltration (Fig. 4e) and cellular replication (Fig. 4f) in the lesion–islet microenvironment.

Fig. 5 Increase in Ki-67 proliferation index but lack of proliferating alpha and beta cells in the PanIN–islet complex. (**a**) Cell proliferation in lesion–islet complex (representative image). The Ki-67$^+$ nuclei (small yellow dots) are labelled with numbers (1 to 40). Blue, insulin; magenta, glucagon; scale bar, 200 μm. Areas around number 10, 12, 28 and 36–39 are enlarged in (**b**) and (**c**). (**b**, **c**) Intra- and peri-islet cell proliferation. Ki-67$^+$ nuclei (arrows, proliferating cells) are seen in the islet mantle and core. They are adjacent to the immunoreactive endocrine cells (glucagon$^+$ or insulin$^+$) but not enclosed by the glucagon or insulin signals. Green, nuclei; scale bar, 50 μm. (**d**, **e**) Proliferating cells adjacent to immunoreactive endocrine cells in duct. This representative view shows that Ki-67$^+$ cells are inside and around duct lesions (white and yellow arrows) but not enclosed by the glucagon or insulin signals. In (**d**) magenta and white arrows highlight a Ki-67$^-$ nucleus (quiescent cell, enclosed by glucagon signal, i.e. immunoreactive alpha cell) alongside a Ki-67$^+$ nucleus (proliferating cell without glucagon or insulin signal). (**d**) and (**e**) are derived from two optical sections (scale bar, 50 μm). (**f**) Increase in Ki-67 proliferation index in lesion–islet complex vs normal pancreatic lobule (>1 mm away from the complex). The index is defined as per cent of cells in proliferation (number of Ki-67$^+$ nuclei/all nuclei in area of interest) ×100%. Nine donor pancreases with the lesion–islet complex were used in the analysis. ***$p < 0.001$. (**g**) Distribution of Ki-67$^+$ proliferating cells in lesion–islet complex. Duct$^{(a)}$ and Duct$^{(b)}$ are the Ki-67$^+$ nuclei in the duct adjacent to (<20 μm) and away from the glucagon or insulin signals, respectively; 530 Ki-67$^+$ nuclei were used in the analysis
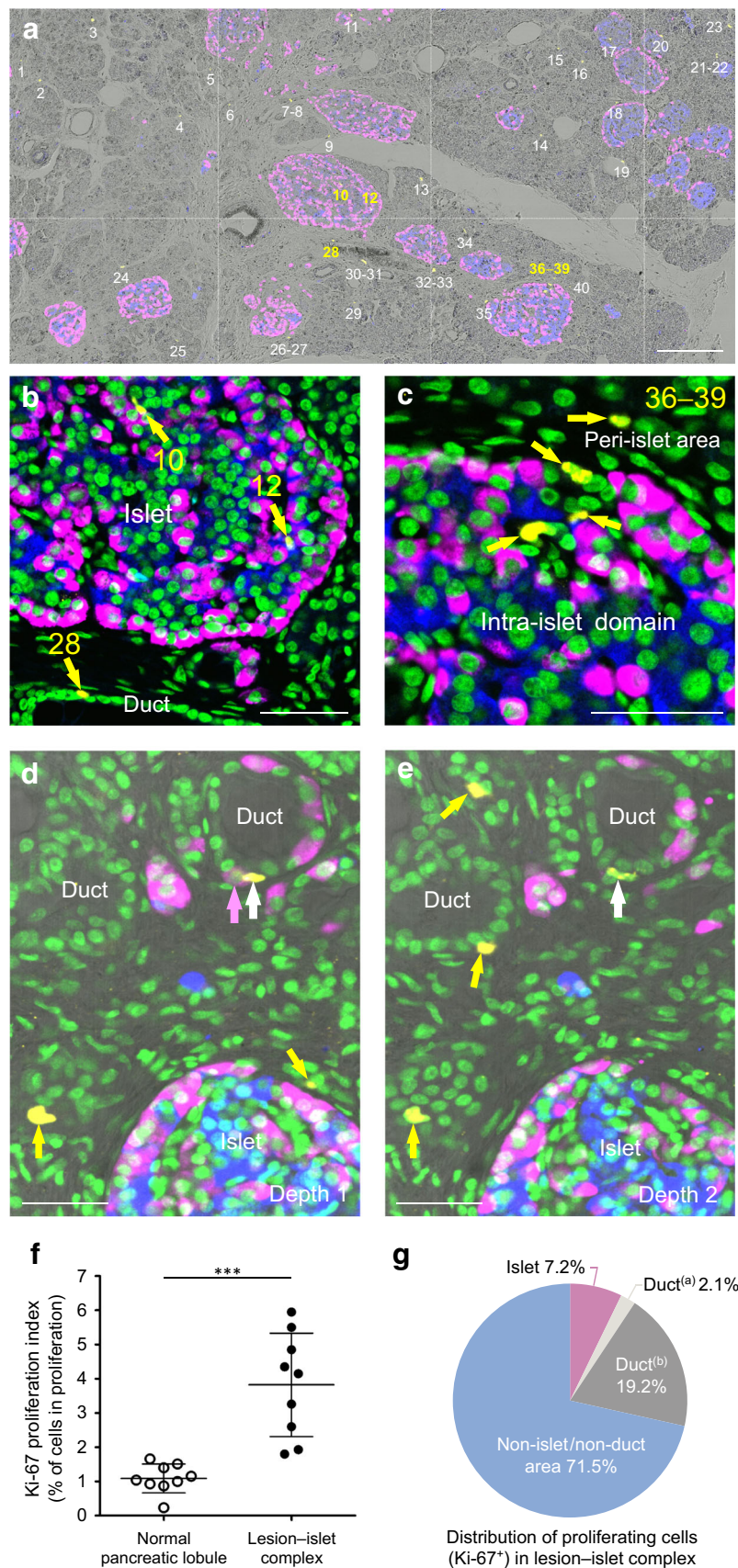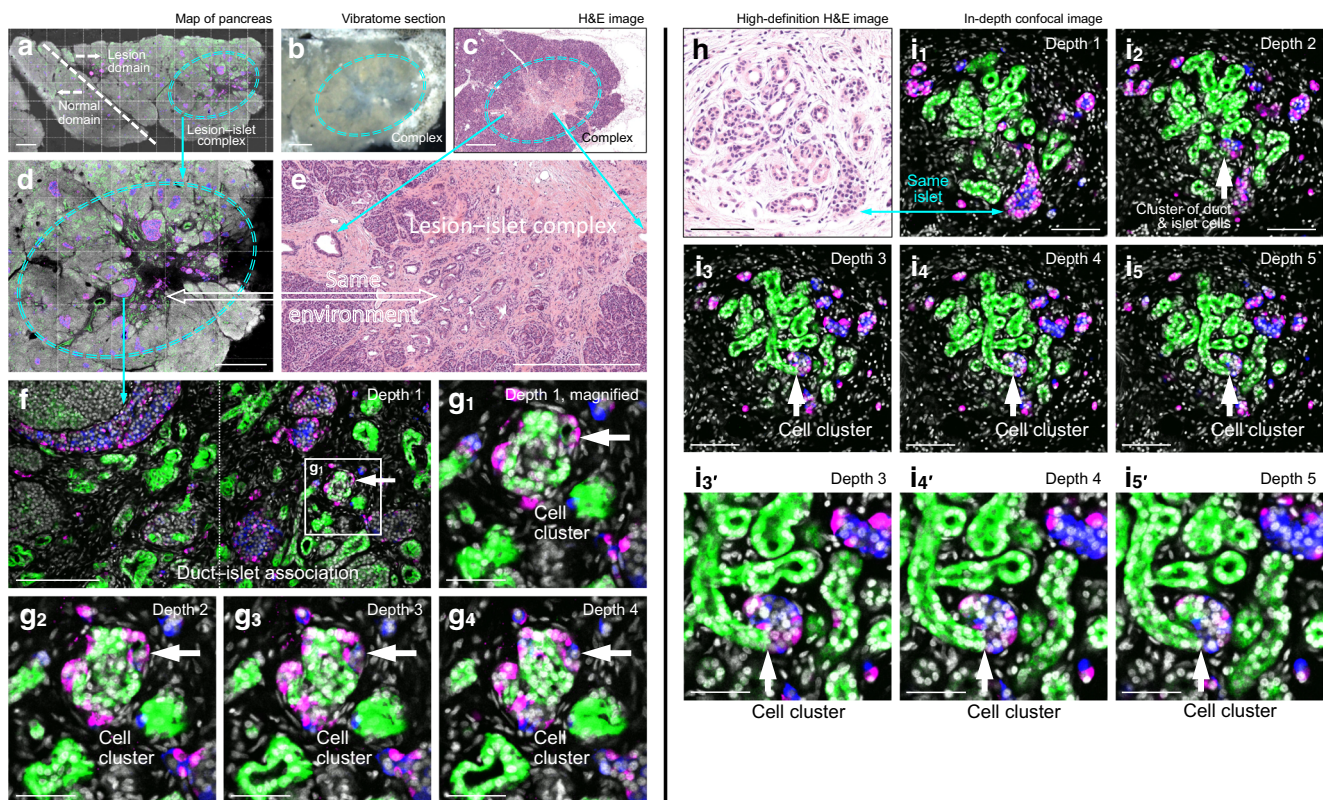
Fig. 6 Formation of duct alpha/beta cell clusters in the PanIN–islet complex. (a–e) Gross view and microenvironment of PanIN–islet complex (representative images). Map of pancreas (a, confocal image), vibratome section of pancreas (b, stereomicroscopic image), and H&E image (c) detect and confirm the islet aggregation (d) and stromal accumulation (e) in the lesion–islet complex (oval). (a) and (c) are enlarged in (d) and (e), respectively (cyan arrows). Magenta, glucagon; blue, insulin; green, CK7; white, nuclei; scale bar in (a–d), 1 mm; scale bar in (e), 500 μm. (f, g) In-depth and continuous contacts of duct and islet cells in cell cluster. The area of interest in (d) is further enlarged in (f; scale bar,

200 μm) to reveal the duct alpha/beta cell cluster (g_1–g_4, white arrows); g_1–g_4 indicate the same cluster at four different focal depths, confirming the cell–cell contacts and integration (scale bar, 50 μm). (h, i) High-resolution H&E and confocal images of duct alpha/beta cell cluster. (h) and (i_{1-5}) (five different focal depths) examine the same PanIN–islet microenvironment (scale bar, 100 μm). The cluster in i_3–i_5 is further enlarged in $i_{3'}$–$i_{5'}$ (scale bar, 50 μm) to confirm the duct–islet cell (glucagon+/insulin+) contacts and integration (arrow). Colours in (f, g, i): magenta, glucagon; blue, insulin; green, CK7; white, nuclei

Pancreatic remodelling in the lesion–islet microenvironment is also reflected by adipocyte association with the lesion–islet complex (Fig. 1a and c). Insulin promotes adipogenesis, in which pre-adipocytes (e.g. stromal cells such as fibroblasts and myofibroblasts) differentiate into adipocytes [35, 36], and stimulates adipocyte proliferation [37]. In Fig. 3, the co-localisation of stromal cells and islets around the PanIN lesion creates favourable conditions to facilitate ectopic fat deposition (also described as pancreatic steatosis or fatty infiltration in the literature [38]). Clinically, both fibrosis and fat replacement of parenchyma are abundant in surgical biopsies for pancreatic cancer [39]. In Figs 1, 3 and 4, we show that the associations among inflammation, fibrosis and fatty infiltration has already manifested in the PanIN–islet microenvironment, highlighting the correlation between the early and late stages of duct lesion progression and the potential pathophysiological impact of the aggregated islets on the perilesional stroma. Regarding the bidirectional relationship between pancreatic cancer and diabetes [40], clinically the

correlation between pancreatic ductal adenocarcinoma and hyperinsulinaemia has long been recognised [41–43]. In our work, the local increase in islet density (Fig. 1a–b) supports the concept that the relationship may have started at the early (PanIN) stage due to the trophic effect of insulin on the exocrine pancreas [44].

In mice, researchers have used the cell tracing technique to investigate beta cell neogenesis in partial duct ligation [12–15]; however, genetic- or chemical-based cell analysis cannot be applied to examine the human pancreas for obvious reasons. Clinically, MRI and endoscopic ultrasound (EUS) are the preferred imaging modalities to detect pancreatic lesions in cancer screening and/or biopsy (e.g. EUS-guided fine-needle aspiration [45]). However, because the two methods cannot resolve cellular structure and identity, their reliability to detect and distinguish PanIN lesions remains questionable [46]. In this research, our measurement of PanIN–islet complexes with an average size at ~3 mm confirms that the associated duct and

islet remodelling at the early stage (i.e. without clinical symptoms) is too small to be resolved by MRI or EUS (resolution at ~1 cm or larger) and thus requires microscopic imaging to detect and confirm pancreatic tissue remodelling. At the microscopic level (100–1000 μm), the PanIN–islet complex, which consists of deformed ducts, aggregated islets and rich stroma (Figs 1, 2 and 3), provides a clear target for detection and immunohistochemical confirmation. This avoids the uncertainty of studying islet remodelling in an undefined environment. However, it should be noted that in 3D human pancreatic histology, false positive and false negative results have both been observed with suboptimal specimens [47]. Artifacts are derived from the residual blood in lobular microvessels (false positive) and light scattering in deep-tissue microscopy (false negative). Therefore, we emphasise the importance of using multiplex signals, including transmitted light (identification of pancreatic lobular structure and fatty infiltration), multi-channel fluorescence (alpha, beta and ductal cell labelling) and H&E staining (PanIN and stroma confirmation) signals, to cross-validate the imaging results acquired from the novel human PanIN–islet microenvironment.

In conclusion, using multiplex signals, we identify and confirm the PanIN–islet complex with intra-islet ducts and duct–islet (alpha/beta) cell clusters in the adult human pancreas. Tissue remodelling and evidence of inflammation, stromal accumulation, and increase in cell replication suggest that the PanIN–islet complex is derived from tissue repair after a local injury. The human PanIN–islet complex thus provides the morphological context for future genetic and/or molecular marker analyses to investigate local islet remodelling involving probable alpha and beta cell neogenesis in a clinically related setting.

Contribution statement All authors contributed to the study concept and design; Y-WT, T-CC, C-YL, C-CC and Y-MJ contributed to human pancreas acquisition and preparation; H-JC, S-JP, M-HC, Y-HC, F-TH, and S-CT contributed to 3D multiplex histology and image presentation; and Y-WT and S-CT contributed to drafting of the manuscript. Y-WT and S-CT obtained funding. All authors contributed to data analysis and interpretation of data, revised the manuscript critically for intellectual content, and approved the final version of the manuscript. S-CT is the guarantor of this work and, as such, had full access to all the data in the study and takes responsibility for the integrity of the data and the accuracy of the data analysis.

References

1. Saisho Y, Butler AE, Manesso E, Elashoff D, Rizza RA, Butler PC (2013) β-Cell mass and turnover in humans: effects of obesity and aging. Diabetes Care 36(1):111–117

2. Hruban RH, Adsay NV, Albores-Saavedra J et al (2001) Pancreatic intraepithelial neoplasia: a new nomenclature and classification system for pancreatic duct lesions. Am J Surg Pathol 25(5):579–586. https://doi.org/10.1097/00000478-200105000-00003

3. Hruban RH, Maitra A, Goggins M (2008) Update on pancreatic intraepithelial neoplasia. Int J Clin Exp Pathol 1(4):306–316

4. Andea A, Sarkar F, Adsay VN (2003) Clinicopathological correlates of pancreatic intraepithelial neoplasia: a comparative analysis of 82 cases with and 152 cases without pancreatic ductal adenocarcinoma. Mod Pathol 16(10):996–1006. https://doi.org/10.1097/01.MP.0000087422.24733.62

5. Detlefsen S, Sipos B, Feyerabend B, Kloppel G (2005) Pancreatic fibrosis associated with age and ductal papillary hyperplasia. Virchows Arch 447(5):800–805. https://doi.org/10.1007/s00428-005-0032-1

6. Lin PY, Peng SJ, Shen CN, Pasricha PJ, Tang SC (2016) PanIN-associated pericyte, glial, and islet remodeling in mice revealed by 3D pancreatic duct lesion histology. Am J Physiol Gastrointest Liver Physiol 311(3):G412–G422. https://doi.org/10.1152/ajpgi.00071.2016

7. Habbe N, Shi G, Meguid RA et al (2008) Spontaneous induction of murine pancreatic intraepithelial neoplasia (mPanIN) by acinar cell targeting of oncogenic Kras in adult mice. Proc Natl Acad Sci U S A 105(48):18913–18918

8. Collins MA, Pasca di Magliano M (2013) Kras as a key oncogene and therapeutic target in pancreatic cancer. Front Physiol 4:407. https://doi.org/10.3389/fphys.2013.00407

9. Zhu L, Shi G, Schmidt CM, Hruban RH, Konieczny SF (2007) Acinar cells contribute to the molecular heterogeneity of pancreatic intraepithelial neoplasia. Am J Pathol 171(1):263–273. https://doi.org/10.2353/ajpath.2007.061176

10. Abraham SC, Wilentz RE, Yeo CJ et al (2003) Pancreaticoduodenectomy (Whipple resections) in patients without malignancy: are they all 'chronic pancreatitis'? Am J Surg Pathol 27(1):110–120. https://doi.org/10.1097/00000478-200301000-00012

11. Cai Y, Yuchi Y, De Groef S et al (2014) IL-6-dependent proliferation of alpha cells in mice with partial pancreatic-duct ligation. Diabetologia 57(7):1420–1427. https://doi.org/10.1007/s00125-014-3242-8

12. Van de Casteele M, Leuckx G, Baeyens L et al (2013) Neurogenin 3+ cells contribute to beta-cell neogenesis and proliferation in injured adult mouse pancreas. Cell Death Dis 4:e523. https://doi.org/10.1038/cddis.2013.52

13. Van de Casteele M, Leuckx G, Cai Y et al (2014) Partial duct ligation: β-cell proliferation and beyond. Diabetes 63(8):2567–2577. https://doi.org/10.2337/db13-0831

14. Xiao X, Chen Z, Shiota C et al (2013) No evidence for beta cell neogenesis in murine adult pancreas. J Clin Invest 123(5):2207–2217. https://doi.org/10.1172/JCI66323

15. Rankin MM, Wilbur CJ, Rak K, Shields EJ, Granger A, Kushner JA (2013) β-Cells are not generated in pancreatic duct ligation-induced injury in adult mice. Diabetes 62(5):1634–1645. https://doi.org/10.2337/db12-0848

16. Dolensek J, Rupnik MS, Stozer A (2015) Structural similarities and differences between the human and the mouse pancreas. Islets 7(1):e1024405. https://doi.org/10.1080/19382014.2015.1024405

17. Cabrera O, Berman DM, Kenyon NS, Ricordi C, Berggren PO, Caicedo A (2006) The unique cytoarchitecture of human pancreatic islets has implications for islet cell function. Proc Natl Acad Sci U S A 103(7):2334–2339

18. Wang P, Fiaschi-Taesch NM, Vasavada RC, Scott DK, Garcia-Ocana A, Stewart AF (2015) Diabetes mellitus–advances and challenges in human beta-cell proliferation. Nat Rev Endocrinol 11(4):201–212. https://doi.org/10.1038/nrendo.2015.9

19. Tang SC, Peng SJ, Chien HJ (2014) Imaging of the islet neural network. Diabetes Obes Metab 16(Suppl 1):77–86

20. Chien HJ, Peng SJ, Hua TE, Kuo CH, Juang JH, Tang SC (2016) 3-D imaging of islets in obesity: formation of the islet-duct complex and neurovascular remodeling in young hyperphagic mice. Int J Obes 40(4):685–697. https://doi.org/10.1038/ijo.2015.224

21. Tang SC, Shen CN, Lin PY et al (2018) Pancreatic neuro-insular network in young mice revealed by 3D panoramic histology. Diabetologia. 61(1):158–167. https://doi.org/10.1007/s00125-017-4408-y

22. Tang SC, Baeyens L, Shen CN (2018) Human pancreatic neuro-insular network in health and fatty infiltration. Diabetologia 61(1):168–181. https://doi.org/10.1007/s00125-017-4409-x

23. Butterworth E, Dickerson W, Vijay V et al (2018) High resolution 3D imaging of the human pancreas neuro-insular network. J Vis Exp 131:e56859

24. Dybala MP, Kuznetsov A, Motobu M et al (2020) Integrated pancreatic blood flow: bidirectional microcirculation between endocrine and exocrine pancreas. Diabetes 69(7):1439–1450. https://doi.org/10.2337/db19-1034

25. Fowler JL, Lee SS, Wesner ZC, Olehnik SK, Kron SJ, Hara M (2018) Three-dimensional analysis of the human pancreas. Endocrinology 159(3):1393–1400. https://doi.org/10.1210/en.2017-03076

26. Alvarsson A, Jimenez-Gonzalez M, Li R (2020) A 3D atlas of the dynamic and regional variation of pancreatic innervation in diabetes. Sci Adv 6(41):eaaz9124. https://doi.org/10.1126/sciadv.aaz9124

27. Juang JH, Peng SJ, Kuo CH, Tang SC (2014) Three-dimensional islet graft histology: panoramic imaging of neural plasticity in sympathetic reinnervation of transplanted islets under the kidney capsule. Am J Physiol Endocrinol Metab 306(5):E559–E570. https://doi.org/10.1152/ajpendo.00515.2013

28. Brune K, Abe T, Canto M et al (2006) Multifocal neoplastic precursor lesions associated with lobular atrophy of the pancreas in patients having a strong family history of pancreatic cancer. Am J Surg Pathol 30(9):1067–1076

29. Masamune A, Watanabe T, Kikuta K, Shimosegawa T (2009) Roles of pancreatic stellate cells in pancreatic inflammation and fibrosis. Clin Gastroenterol Hepatol 7(11 Suppl):S48–S54. https://doi.org/10.1016/j.cgh.2009.07.038

30. Apte MV, Wilson JS, Lugea A, Pandol SJ (2013) A starring role for stellate cells in the pancreatic cancer microenvironment. Gastroenterology 144:1210–1219. https://doi.org/10.1053/j.gastro.2012.11.037

31. Pour PM (1997) The role of Langerhans islets in pancreatic ductal adenocarcinoma. Front Biosci 2:d271–d282. https://doi.org/10.2741/A190

32. Pour PM, Pandey KK, Batra SK (2003) What is the origin of pancreatic adenocarcinoma? Mol Cancer 2(13):1–10

33. El-Gohary Y, Wiersch J, Tulachan S et al (2016) Intraislet pancreatic ducts can give rise to insulin-positive cells. Endocrinology. 157(1):166–175. https://doi.org/10.1210/en.2015-1175

34. Hill DJ, Milner RD (1985) Insulin as a growth factor. Pediatr Res 19(9):879–886. https://doi.org/10.1203/00006450-198509000-00001

35. Sorisky A (1999) From preadipocyte to adipocyte: differentiation-directed signals of insulin from the cell surface to the nucleus. Crit Rev Clin Lab Sci 36(1):1–34

36. Klemm DJ, Leitner JW, Watson P (2001) Insulin-induced adipocyte differentiation. Activation of CREB rescues adipogenesis from the arrest caused by inhibition of prenylation. J Biol Chem 276(30):28430–28435. https://doi.org/10.1074/jbc.M103382200

37. Geloen A, Collet AJ, Guay G, Bukowiecki LJ (1989) Insulin stimulates in vivo cell proliferation in white adipose tissue. Am J Phys 256(1 Pt 1):C190–C196

38. Smits MM, van Geenen EJ (2011) The clinical significance of pancreatic steatosis. Nat Rev Gastroenterol Hepatol 8(3):169–177. https://doi.org/10.1038/nrgastro.2011.4

39. Hori M, Takahashi M, Hiraoka N et al (2014) Association of pancreatic fatty infiltration with pancreatic ductal adenocarcinoma. Clin Transl Gastroenterol 5:e53. https://doi.org/10.1038/ctg.2014.5

40. Sah RP, Nagpal SJ, Mukhopadhyay D, Chari ST (2013) New insights into pancreatic cancer-induced paraneoplastic diabetes. Nat Rev Gastroenterol Hepatol 10:423–433. https://doi.org/10.1038/nrgastro.2013.49

41. Permert J, Adrian TE, Jacobsson P, Jorfelt L, Fruin AB, Larsson J (1993) Is profound peripheral insulin resistance in patients with pancreatic cancer caused by a tumor-associated factor? Am J Surg 165:61–66; discussion 66–67. https://doi.org/10.1016/S0002-9610(05)80405-2

42. Hart PA, Bellin MD, Andersen DK et al (2016) Type 3c (pancreatogenic) diabetes mellitus secondary to chronic pancreatitis and pancreatic cancer. Lancet Gastroenterol Hepatol 1:226–237. https://doi.org/10.1016/S2468-1253(16)30106-6

43. Abbruzzese JL, Andersen DK, Borrebaeck CAK et al (2018) The interface of pancreatic cancer with diabetes, obesity, and inflammation: research gaps and opportunities: summary of a National Institute of Diabetes and Digestive and Kidney Diseases Workshop. Pancreas 47:516–525. https://doi.org/10.1097/MPA.0000000000001037

44. Henderson JR, Daniel PM, Fraser PA (1981) The pancreas as a single organ: the influence of the endocrine upon the exocrine part of the gland. Gut 22:158–167. https://doi.org/10.1136/gut.22.2.158

45. Hewitt MJ, McPhail MJ, Possamai L, Dhar A, Vlavianos P, Monahan KJ (2012) EUS-guided FNA for diagnosis of solid pancreatic neoplasms: a meta-analysis. Gastrointest Endosc 75(2):319–331. https://doi.org/10.1016/j.gie.2011.08.049

46. Aslanian HR, Lee JH, Canto MI (2020) AGA clinical practice update on pancreas cancer screening in high-risk individuals: expert review. Gastroenterology 159(1):358–362. https://doi.org/10.1053/j.gastro.2020.03.088

47. Chien HJ, Chiang TC, Peng SJ et al (2019) Human pancreatic afferent and efferent nerves: mapping and 3-D illustration of exocrine, endocrine, and adipose innervation. Am J Physiol Gastrointest Liver Physiol 317(5):G694–G706. https://doi.org/10.1152/ajpgi.00116.2019